



# CHALMERS

## Chalmers Publication Library

### **High-Speed 850 nm Quasi-Single Mode VCSELs for Extended Reach Optical Interconnects**

This document has been downloaded from Chalmers Publication Library (CPL). It is the author's version of a work that was accepted for publication in:

**Journal of Optical Communications and Networking (ISSN: 1943-0620)**

Citation for the published paper:

Safaisini, R. ; Szczerba, K. ; Westbergh, P. et al. (2013) "High-Speed 850 nm Quasi-Single Mode VCSELs for Extended Reach Optical Interconnects". Journal of Optical Communications and Networking, vol. 5(7), pp. 686-695.

Downloaded from: <http://publications.lib.chalmers.se/publication/180424>

Notice: Changes introduced as a result of publishing processes such as copy-editing and formatting may not be reflected in this document. For a definitive version of this work, please refer to the published source. Please note that access to the published version might require a subscription.

Chalmers Publication Library (CPL) offers the possibility of retrieving research publications produced at Chalmers University of Technology. It covers all types of publications: articles, dissertations, licentiate theses, masters theses, conference papers, reports etc. Since 2006 it is the official tool for Chalmers official publication statistics. To ensure that Chalmers research results are disseminated as widely as possible, an Open Access Policy has been adopted. The CPL service is administrated and maintained by Chalmers Library.

(article starts on next page)

# High-Speed 850-nm Quasi-Single Mode VCSELs for Extended Reach Optical Interconnects

Rashid Safaisini, Krzysztof Szczerba, Petter Westbergh, Erik Haglund, Benjamin Kögel, Johan S. Gustavsson, Anders Larsson, Magnus Karlsson, and Peter Andrekson

**Abstract**— This paper presents recent results on high-speed, quasi-single mode, 850-nm vertical-cavity surface-emitting lasers (VCSELs) with a narrow spectral width for extended reach optical interconnects. The top mirror reflectivity is adjusted for high output power, slope efficiency, and modulation bandwidth (3 dB cut-off frequency). An oxide confined VCSEL with a  $\sim 3 \mu\text{m}$  aperture diameter delivers 2 mW of output power and reaches a resonance frequency as high as 25 GHz and a modulation bandwidth exceeding 20 GHz. A small K-factor of 0.17 ns and a large D-factor of 17.3 GHz/mA<sup>1/2</sup>, extracted from the VCSEL modulation response, along with the improved DC and modal properties enable energy-efficient data transmission at high bit-rates over long distance multimode fiber. Error-free transmission at bit-rates exceeding 20 Gb/s over 1.1 km of OM4 fiber is demonstrated and shown to be limited mainly by the photoreceiver bandwidth. A theoretical investigation of the dependence of link performance on photoreceiver bandwidth is also presented.

**Index Terms**— High-speed data communication; long distance data transmission; multi-mode fiber; narrow spectral width; optical interconnect; quasi-single mode laser; vertical-cavity surface-emitting laser (VCSEL).

## I. INTRODUCTION

The demand for high-speed optical data communication is perpetually growing in our modern Internet era, due to the need for fast access to large amounts of information. This technology trend not only requires an increase of the link speed to 20-25 Gb/s, but also an extension of the interconnect length up to 2 km for intra-building links in office areas and data centers [1,2]. Owing to their unique properties, vertical-cavity surface-emitting lasers (VCSELs) have already been a part of multiple standards and are widely deployed in applications such as

optical links and networks in data centers and high performance computing systems [3,4]. The combination of 850 nm VCSELs and multi-mode fibers (MMFs) has been the best solution for short-reach high-speed optical interconnects for several years [4,5]. Even though single-mode fibers (SMFs) with long wavelength lasers (1310 nm and 1550 nm) is a proven solution for >10 km links, MMF links at 850 nm are more cost-efficient for extended short-reach interconnects (up to  $\sim 2$  km) due to more tolerant optical alignment and lower cost optoelectronic components, assembly, and packaging. Although the price per km of MMFs is higher than for SMFs.

One of the main challenges of high bit-rate transmission over long MMFs arises from the limited bandwidth caused by effects of chromatic dispersion (mainly due to material dispersion) and modal dispersion (depending on the fiber refractive index profile). However, in new generations of MMFs, the chromatic dispersion can be compensated by modal dispersion by proper index profiling for a left-tilted differential mode delay specification [6]. Employing this technique, MMFs with an effective modal bandwidth exceeding 4700 MHz·km (OM4 fiber) are already introduced to increase the reach of 10 Gb Ethernet from 300 to 550 m [7]. Moreover, improving VCSEL modal properties to reduce the number of transverse optical modes, and consequently the emission spectral width, is crucial for reducing the effects of chromatic dispersion and achieving even longer transmission distance [8]. In addition to improved modal properties, VCSELs utilized in high bit-rate and long reach applications should meet at least two more requirements: improved speed to increase the total bandwidth of the link and improved optical output power to overcome optical penalties and losses and reach the required received power for error-free detection. A compromise may need to be considered to reach the best performance for a particular bit-rate and fiber length since simultaneous achievement of all three requirements might be challenging.

Large efforts have been devoted to increasing the bit-rate and/or the distance at error-free transmission (defined as bit-error rate (BER)  $< 10^{-12}$ ) over MMF using directly modulated 850-nm VCSELs [8-16]. Record bit-rates of 47 Gb/s back-to-back (BTB) and 44 Gb/s over 50 m of MMF, using a VCSEL with a 27 GHz modulation bandwidth, was recently reported by reducing the mirror resistances and employing a short cavity for improved carrier transport and optical confinement [9]. Moreover, various attempts focused on increasing the transmission distance by utilizing narrow spectral width VCSELs,

Manuscript received December 28, 2012. This work was supported by the Swedish Foundation for Strategic Research (SSF).

R. Safaisini, K. Szczerba, P. Westbergh, E. Haglund, B. Kögel, J. S. Gustavsson, A. Larsson, M. Karlsson, and P. Andrekson are with the Photonics Laboratory at the Department of Microtechnology and Nanoscience, Chalmers University of Technology, Göteborg 412 96 Sweden. (e-mail: rashid.safaisini@chalmers.se).

either by employing an integrated mode filter to suppress higher order modes or a small oxide aperture to support a smaller number of lasing modes. Data transmission over 500 m of MMF at 25 Gb/s was reported using a VCSEL with a 5  $\mu\text{m}$  oxide aperture and an integrated mode filter [10] and also a VCSEL with  $\sim 3 \mu\text{m}$  oxide aperture [11]. Small aperture VCSELs offer a less complex approach for the required modal properties and have proved to be more energy efficient than large aperture VCSELs, as investigated by a group at TU Berlin [12], due to improved dynamics related to their small cavity volume, although there might be some concerns about their reliability [17]. There have been reports on 25 Gb/s transmission over 300 [13] and 603 m [14] of MMF using quasi-single mode (side mode suppression ratio (SMSR)  $\sim 20$  dB) VCSELs with a  $\sim 3\text{-}4 \mu\text{m}$  aperture diameter. The highest bit-rate achieved at longer distance is 20 Gb/s over 1100 m, which was also accomplished using a small aperture, quasi-single mode VCSEL [15]. The highest bit-rate–distance product was reported in [16], where transmission at 10 Gb/s over 2.8 km of high bandwidth MMF was demonstrated using a single mode VCSEL.

This paper presents results from our recent work on small aperture, narrow spectral width, quasi-single mode VCSELs with a modulation bandwidth exceeding 20 GHz. This has enabled transmission at bit-rates exceeding 20 Gb/s over more than 1 km of OM4 MMF with low energy dissipation. The top distributed Bragg reflector (DBR) reflectivity was reduced [18] for low damping of the modulation response, high slope efficiency, and high output power to meet requirements in terms of speed, modulation efficiency, and received optical power. To the best of the authors' knowledge, this represents state-of-the-art for transmission at high bit-rates over more than 1 km of MMF using a directly modulated VCSEL.

## II. VCSEL DESIGN AND FABRICATION

### A. Structure

The epitaxial structure is grown by metal-organic vapor phase epitaxy on an undoped GaAs substrate. The n-type (Si-doped,  $\sim 2\text{-}6 \times 10^{18} \text{ cm}^{-3}$ ) DBR contains 28 pairs of AlAs/Al<sub>0.12</sub>Ga<sub>0.88</sub>As at the lower part, followed by three pairs of Al<sub>0.90</sub>Ga<sub>0.10</sub>As/Al<sub>0.12</sub>Ga<sub>0.88</sub>As on top and just below the cavity. Utilizing the high thermal conductivity binary compound AlAs facilitates efficient vertical heat transport from the active region through the bottom DBR and therefore reduces the thermal resistance. This is of particular importance in small aperture VCSELs which usually suffer from thermal issues more than large aperture ones.

The active region employs five 4-nm-thick In<sub>0.10</sub>Ga<sub>0.90</sub>As quantum wells (QWs) separated by 6-nm Al<sub>0.37</sub>Ga<sub>0.63</sub>As barriers. Incorporating indium in the QWs results in increased differential gain through strain-induced valence band splitting and enhanced quantum size effects [19]. The top DBR is formed by 23 pairs of p-type (C-doped,  $\sim 2\text{-}3 \times 10^{18} \text{ cm}^{-3}$ ) Al<sub>0.90</sub>Ga<sub>0.10</sub>As/Al<sub>0.12</sub>Ga<sub>0.88</sub>As. Two 30-nm-thick Al<sub>0.98</sub>Ga<sub>0.02</sub>As layers were introduced in the top DBR right above the cavity to allow for wet oxidation during device processing and for defining the current and optical aperture. Four additional 30-nm-thick

AlGaAs oxide layers with 96% Al-content are placed above the two high Al-content oxide layers to reduce the parasitic oxide capacitance.

### B. VCSEL Fabrication

The VCSELs were fabricated through a sequence of standard high-speed VCSEL processing steps including mesa formation, metal contact deposition, wet oxidation, and planarization. The fabrication started by sputter deposition of a Ti/Au ring metal contact on a highly doped GaAs cap layer. Then, VCSEL mesas with 22, 24, 26, and 28  $\mu\text{m}$  diameter were defined by dry etching of the patterned surface using an inductively coupled plasma (ICP) system with SiCl<sub>4</sub>/Ar and Cl<sub>2</sub>/Ar gas mixtures. The etching was precisely stopped at the desired position above AlAs layers by in-situ optical etch depth monitoring. After mesa etching, the sample was covered by SiN<sub>x</sub> using plasma-enhanced chemical-vapor deposition to avoid surface oxidation during the wet oxidation process. This step was followed by removal of the SiN<sub>x</sub> on the mesa sidewalls by NF<sub>3</sub> plasma etching and definition of the oxide aperture using selective wet oxidation at 420 °C. The oxidation process was monitored by an IR microscope to form small, 2-4  $\mu\text{m}$  aperture, VCSELs with 22  $\mu\text{m}$  diameter mesas for (quasi) single-mode operation with  $>1$  mW output power. In the next step, a deeper mesa with 50  $\mu\text{m}$  diameter was etched down to a 1- $\mu\text{m}$  thick n-contact layer below the n-DBR using the ICP system and similar gas mixtures as used for the shallow mesa etch. The larger mesa diameter at the bottom facilitates heat transport from the active region through the bottom DBR. An electron-beam evaporated Ni/Ge/Au contact was then deposited on the highly doped ( $\sim 4 \times 10^{18} \text{ cm}^{-3}$ ) contact layer as an n-type contact followed by lift-off and contact annealing at 420 °C in an N<sub>2</sub> environment to reduce the contact resistivity. Before VCSEL planarization with benzocyclobutene (BCB), the contact layer under the signal bondpad was etched away to minimize the pad capacitance. The VCSEL fabrication was finished by sputter deposition of a Ti/Au bondpad on the BCB to form a ground-signal-ground (GSG) contact configuration for device measurement. The completed VCSEL is schematically illustrated in Fig. 1. To boost the output power, slope efficiency, and speed of the VCSELs, the reflectivity of the output coupling DBR was adjusted by shallow ICP etching of the top mesa surface [18] using a SiCl<sub>4</sub>/Ar gas mixture and 50 W RF power. This step, with  $\sim 50$  nm etch depth, led to an approximately 40% increase of the maximum output power and the slope efficiency with only a slight increase in threshold current. Having a high launched optical power is essential to compensate for fiber and connector losses for transmission over long fibers.

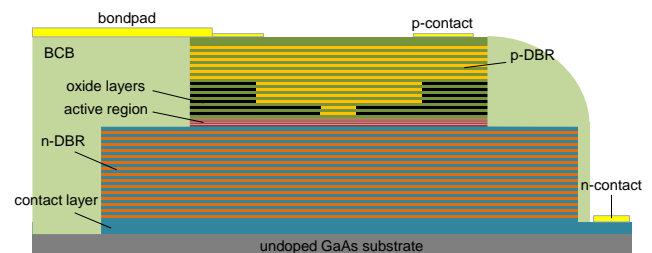


Fig. 1 A cross-section view of the fabricated VCSEL.

### III. VCSEL CHARACTERIZATION

#### A. DC Measurements

The light output power-current-voltage (LIV) characteristics of a  $\sim 3 \mu\text{m}$  oxide aperture diameter VCSEL at  $20^\circ\text{C}$  after top mirror reflectivity adjustment are presented in Fig. 2. The VCSEL has a threshold current of 0.19 mA, a 44% differential quantum efficiency, and a  $\sim 230 \Omega$  differential resistance. The output power measured by a calibrated large area silicon photodetector is 2 mW at the thermal roll-over current of 5.7 mA. The VCSEL operates primarily in the fundamental mode with an SMSR of 33, 22, and 18 dB at 1, 2, and 2.7 mA, respectively. The corresponding RMS spectral widths ( $\Delta\lambda_{\text{rms}}$ ) are 0.18, 0.21, and 0.29 nm. These values are well below the required  $\Delta\lambda_{\text{rms}}=0.45 \text{ nm}$  for IEEE standards [19] and stay below that for up to 5 mA bias current. The optical emission spectra of the VCSEL at different bias currents are shown in Fig. 3. The optical spectra under modulation do not show any remarkable difference from the presented DC spectra. The reduced VCSEL spectral width directly reduces the effects of chromatic fiber dispersion while it also reduces the effects of modal dispersion since the quasi-single mode VCSEL excites a reduced number of fiber modes. This leads to a higher effective fiber bandwidth, which enables a longer transmission distance, assuming no connectors or bends in the fiber causing redistribution of the modes.

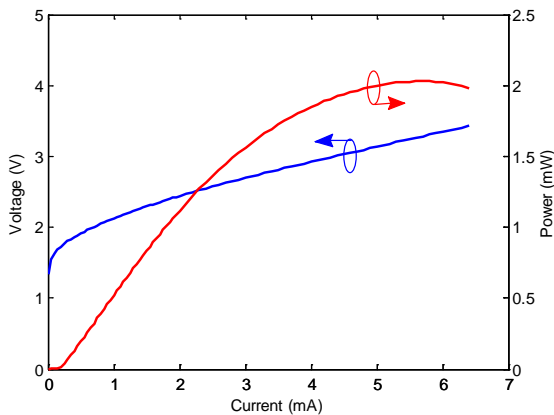


Fig. 2 LIV characteristics of the  $\sim 3 \mu\text{m}$  aperture VCSEL.

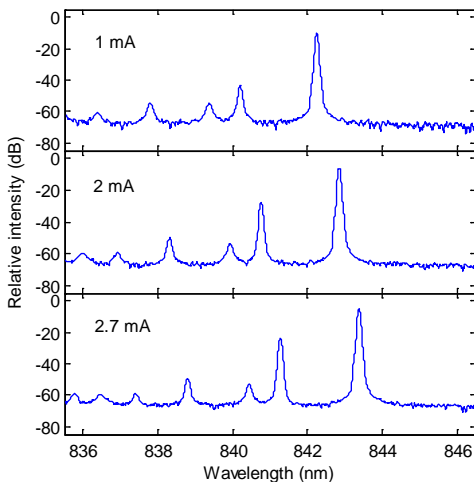


Fig. 3 Optical spectra of the  $\sim 3 \mu\text{m}$  aperture VCSEL at 1, 2, and 2.7 mA.

The DC characteristics suggest that this VCSEL meets the modal properties and power requirements for long distance MMF transmission. The required output power at modulation current for a 1 km MMF link at a data-rate of  $\sim 20 \text{ Gb/s}$  can be estimated to be  $\sim 1\text{-}2 \text{ mW}$ , accounting for 50% coupling loss, 2.2 dB/km fiber loss (for OM4 fiber), 0.5 dB loss per connector, and a -6 dBm receiver sensitivity for error-free detection.

#### B. AC Characterization

A modulation bandwidth of 23 GHz was already reported for a  $7 \mu\text{m}$  aperture diameter VCSEL with the same epitaxial design and optimized photon lifetime [21]. The frequency response of the  $\sim 3 \mu\text{m}$  aperture VCSEL was measured using a 65 GHz Anritsu 3797C vector network analyzer and a GaAs 1481 pin photodetector from New Focus with 25 GHz bandwidth and a responsivity of  $0.4 \text{ A/W}$  at 850 nm. The measured response is then corrected for the frequency responses of the photodetector and the high speed GSG probe. The modulation responses of the VCSEL, depicted in Fig. 4 for different bias currents, show a maximum 3 dB frequency of 21 GHz. The low frequency roll-off observed in the modulation response, particularly at low bias currents, can be attributed to the effects of spatial hole burning in the active region [22]. A second order system transfer function derived from the single-mode rate equations, with an additional pole accounting for the effects of electrical parasitics and carrier transport with a cut-off frequency  $f_p$  (Eq. 1) [23], is then fitted to the modulation responses in Fig. 4.

$$H(f) = \text{const} \times \frac{f_r^2}{f_r^2 - f^2 + j(f/2\pi)\gamma} \times \frac{1}{1 + j(f/f_p)} \quad (1)$$

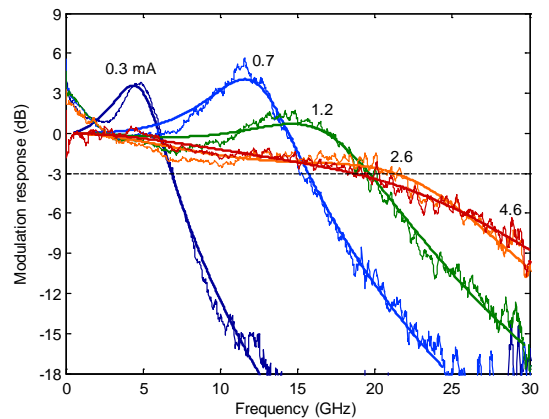


Fig. 4 Modulation response of the VCSEL under test at different bias currents.

The transfer function,  $H(f)$ , is used to extract the relaxation resonance frequency,  $f_r$ , and the damping factor,  $\gamma$ , for each bias current. The damping factor can be written as a function of resonance frequency squared,  $\gamma=K f_r^2+\gamma_0$ , where the K-factor describes the rate at which damping increases with resonance frequency and  $\gamma_0$  is the damping factor offset [24] which is important at low bias currents where  $f_r$  is small. Fig. 5 shows a plot of  $\gamma$  as a function of  $f_r^2$  and the linear fit that determines the K-factor and the damping offset to be  $0.17 \text{ ns}^{-1}$  and  $6.8 \text{ ns}^{-1}$ , respectively. Such a small K-factor yields values exceeding 50 GHz for the damping-limited maximum modulation bandwidth which can be expressed as

$f_{3dB,damping} \approx 2\pi\sqrt{2/K}$  [24]. A small K-factor, and thus small damping, is essential for realizing high modulation bandwidth VCSELs. However, a certain amount of damping is needed to prevent excessive ringing and timing jitter. Therefore, there is an optimum amount of damping for a given bit-rate.

The D-factor, which describes how fast  $f_r$  increases with increasing bias current,  $I$ , above the threshold current,  $I_{th}$ ,  $f_r = D \cdot (I - I_{th})^{1/2}$ , is another parameter of importance for the VCSEL dynamics. Achieving high resonance frequencies at low bias currents, and therefore a large D-factor, is desired for high-speed modulation. A large D-factor is also essential for high energy efficiency at high bit-rates [14] since a high  $f_r$ , and therefore a high modulation bandwidth, can be reached at a lower bias current and voltage. The D-factor can be increased by improving internal quantum efficiency and differential gain, and by reducing the cavity volume [24] through proper epitaxial design and small aperture diameters. A large D-factor and high slope efficiency enable high modulation bandwidth and output power at low bias currents, which lead to low power consumption in high-speed data transmission.

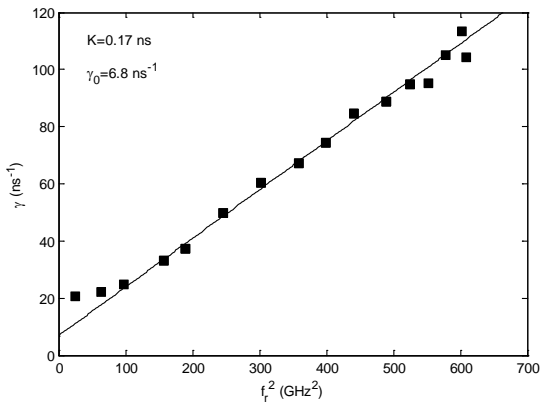


Fig. 5 Damping rate as a function of resonance frequency squared.

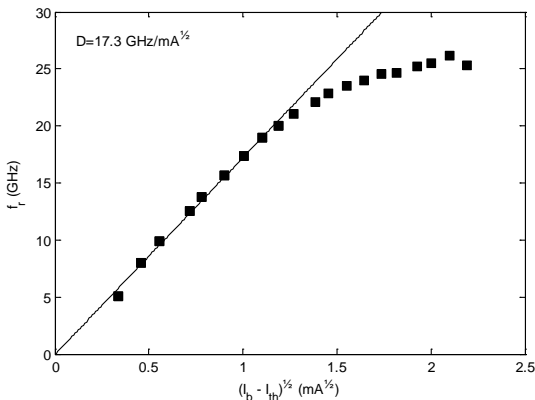


Fig. 6 Resonance frequency as a function of square root of current above threshold.

Fig. 6 presents  $f_r$  as a function of  $(I - I_{th})^{1/2}$  for the VCSEL under test, where  $D$  is estimated from the fit to the linear part of the curve, before reaching thermal saturation at high bias currents. Large values of  $D=17.3 \text{ GHz/mA}^{1/2}$  and  $f_{r,max}=25 \text{ GHz}$  are achieved for this small aperture VCSEL. The maximum 3 dB bandwidth when only considering thermal effects [24] is limited to  $f_{3dB,thermal} \approx 1.55 \cdot f_{r,max} = 39 \text{ GHz}$ , which is well above the 3 dB bandwidth of this VCSEL. Therefore, thermal effects

are not considered a major bandwidth limiting factor for this design. The main bandwidth limitation effect, in fact, was found to be the parasitic electrical elements according to the measured impedance characteristics. This was done by fitting a VCSEL parasitic equivalent-circuit model [25] to the measured  $S_{11}$  data. The RC parasitic cut-off frequency,  $f_{RC}$ , was then estimated from the parasitic elements. This showed that  $11 \text{ GHz} < f_{RC} < 18 \text{ GHz}$  for bias currents between 0.3 and 5 mA ( $f_{RC}=16 \text{ GHz}$  at 2.6 mA bias current). Reducing the mirror resistance and improving the carrier transport to the QWs to reduce the diffusion capacitance have been recently shown to increase the VCSEL 3 dB bandwidth to 28 GHz [26]. Although parasitic cut-off frequency could also be estimated from the fit of the transfer function to the  $S_{21}$  data ( $f_p$ ), the parasitic frequency extracted from  $S_{11}$  data is believed to give a more accurate value ( $f_{RC}$ ). Additionally,  $S_{11}$  data provides quantitative values for each parasitic element, which can be useful for improving the epitaxial design.

### C. Transmission Experiment

The large signal modulation performance of the quasi-single mode VCSEL was evaluated at 20 °C by recording eye diagrams and BERs for BTB and after 500, 800, and 1100 m transmission on Draka MaxCap-OM4 MMF. The measurement set-up for the transmission experiments is shown in Fig. 7.

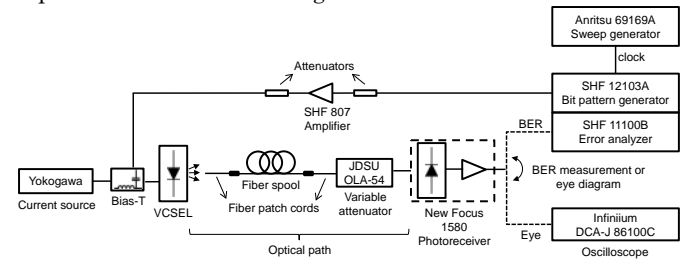


Fig. 7 Measurement set-up for transmission experiments.

A non-return-to-zero data pattern with a  $2^7-1$  bits long pseudorandom binary sequence, generated by an SHF 12103A bit pattern generator, was fed to the VCSEL through a linear SHF 807 amplifier with 24 dB gain in combination with a total of 23 dB attenuation and a 30 GHz SHF 120A bias-T via the GSG high speed probe. The linear amplifier together with the attenuators were employed to suppress unwanted microwave reflections resulting from VCSEL impedance mismatch to 50 Ω. The light output was butt-coupled to a 62.5 μm core diameter MMF which was aligned for ~50% coupling efficiency, before launching to 50 μm core diameter OM4 MMFs. Single fiber spools were used for 500 and 800 m long data transmission whereas the 1100 m long link was made by connecting 300 and 800 m fiber spools. Two additional 1 m OM4 fiber patch cords, with a flat connector (PC) on one end and an angled connector (APC) on the other end, were used to adapt the angled ends of the fiber spools to the flat fiber connectors. The fiber was then connected to a JDSU OLA-54 variable optical attenuator to vary the received optical power at the photoreceiver for the BER measurement. The photoreceiver package used for the transmission experiments contains a New Focus 1580 photodiode, with a nominal bandwidth of 12 GHz and a responsivity of 0.4 A/W at 850 nm, and an integrated

transimpedance amplifier. The actual response of the photoreceiver showed a 3 dB bandwidth of 10 GHz and a 6 dB cut-off frequency of 14 GHz. The use of an integrated amplifier in the photoreceiver package can effectively reduce the noise level and improve the signal quality by better impedance matching for reduced microwave reflections. However, the photoreceiver available at the time of this experiment has a limited bandwidth which affects measurements at high bit-rates. This limit will be addressed in more detail in the next section.

Another 1 m long OM4 patch cord was used to connect the variable attenuator to the optical input of the photoreceiver, while the output electrical signal was used to record eye diagrams using an Agilent Infiniium DCA-J 86100C 70 GHz digital communications analyzer or to perform BER analysis using an SHF 11100B error analyzer. The VCSEL was biased at 2.7 mA (~38 kA/cm<sup>2</sup>) and the peak-to-peak modulation voltage measured at the high-speed probe was 0.95 V for all transmission measurements. The VCSEL reliability at such high current densities needs to be investigated even though the small aperture VCSELs are believed to be able to reliably operate at higher current densities than the large aperture ones [17]. The bias current and the modulation voltage were adjusted to give the best quality eyes. The VCSEL energy dissipation, defined as dissipated power/bit-rate, is 220 fJ/bit for data transmission at 25 Gb/s. Dissipated power was calculated as  $P_{diss}=IV-P_{opt}$ , where  $V$  and  $P_{opt}$  are bias voltage and output power, respectively, at bias current,  $I$ . The record VCSEL energy efficiency of 188 fJ/bit was reported for transmission over 600 m at 25 Gb/s using a ~4 μm oxide aperture quasi-single mode 850 nm VCSEL [14].

Inverted eyes and results from BER measurements for data rates of 20 and 22 Gb/s are shown in Fig. 8 and 9, respectively, for BTB transmission and after transmission over 500, 800, and 1100 m of OM4 MMF. Open eyes and error-free operation were achieved for transmission up to 1100 m at both data rates. However, the eyes at 22 Gb/s for transmission over long lengths of fiber suffer from intersymbol interference (ISI), which limits the transmission distance at data rates exceeding 22 Gb/s. A power penalty of approximately 2 dB is observed when increasing the transmission distance from BTB to 1100 m, at which the received optical power for BER=10<sup>-12</sup> is below -7 dBm at 20 Gb/s and about -6 dBm at 22 Gb/s.

A reduction of the required received optical power is observed at 22 Gb/s when increasing the transmission length from 800 m to 1100 m. This can be attributed to a change in the fiber frequency response due to an improved mode power distribution in the fiber when connecting the 300 and 800 m fiber spools. This effect can alter the ISI, and consequently the system performance, and has been previously studied using an advanced MMF link modeling tool [27]. Despite the reduction of the required received optical power for increasing the fiber length from 800 m to 1100 m at 22 Gb/s bit-rate, the presented eye diagram for 800 m fiber shows a lower jitter and ISI than the one for 1100 m fiber. This discrepancy may be due to sensitivity of link response to fiber configuration and caused by randomly connecting two fiber spools for the 1100 m case, while performing BER and eye diagram measurements. The increased jitter with fiber length for both 20 and 22 Gb/s bit-rates is attributed to the increased effect of fiber dispersion with increased fiber length.

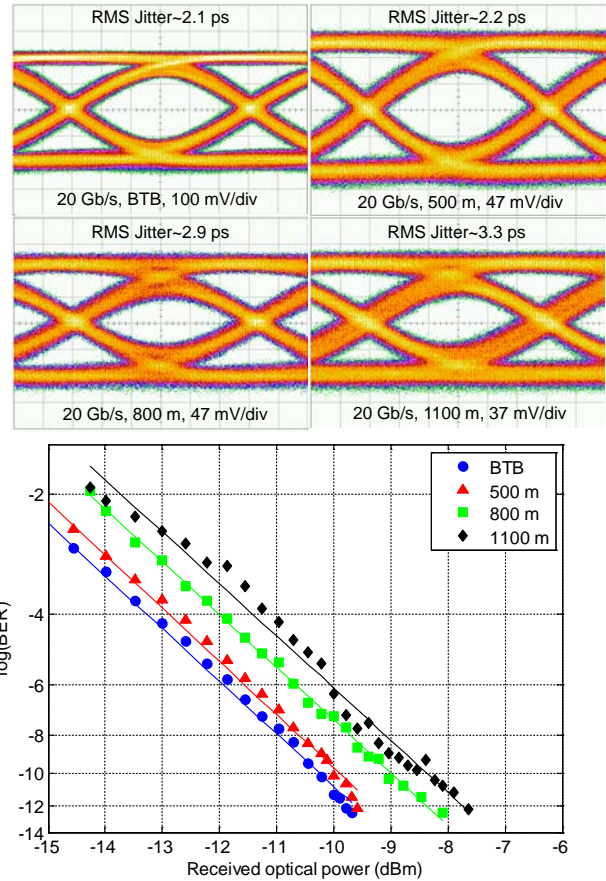


Fig. 8 Eye diagrams and BER measurements for 20 Gb/s data transmission BTB and over 500, 800, and 1100 m of MMF [15].

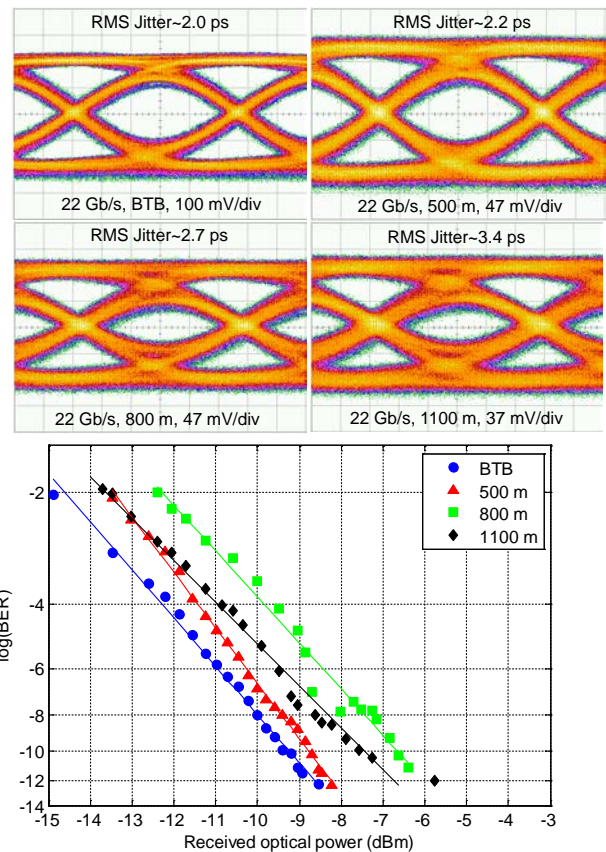


Fig. 9 Eye diagrams and BER measurements for 22 Gb/s data transmission BTB and over 500, 800, and 1100 m of MMF.

Data transmission at 25 Gb/s was performed BTB and with 500 and 800 m MMF to find the upper limit of the transmission capacity with the current set-up. The results, presented in Fig. 10, indicate that even though error-free transmission is achieved BTB and after 500 m of fiber, a higher laser optical power is needed to meet the receiver sensitivity requirement for the 800 m MMF case. Error-free transmission over longer distances of MMF can also be achieved by improving the system bandwidth (which is mainly limited by the bandwidth of the photoreceiver) for reduced ISI and improved receiver sensitivity at this bit-rate.

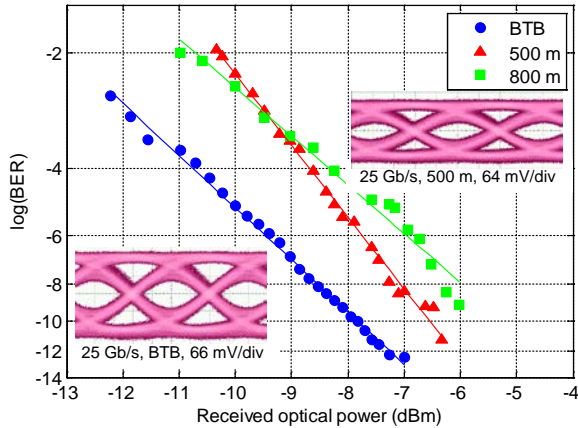


Fig. 10 BER measurements for 25 Gb/s data transmission BTB and over 500 and 800 m of MMF. The insets show the eye diagrams for BTB and over 500 m data transmission.

The nonlinear behavior observed in the measured BER data for longer fibers can be attributed to redefining the center point in the eye while measuring BER at each received power. This behavior will be more pronounced at higher bit-rates and longer fibers where the link experiences more ISI.

#### IV. DISCUSSIONS

To analyze the data transmission results and identify the factors limiting the bit-rate and fiber length, theoretical receiver sensitivities at  $BER=10^{-12}$  were calculated for different bit-rates and fiber lengths. This calculation was performed for the set-up used in the previous section for transmission experiments with the 10 GHz bandwidth receiver, as well as for the same set-up with a theoretical 15 GHz bandwidth receiver instead. The calculations are based on measured frequency responses of the link including a similar VCSEL as reported here along with the 10 GHz photoreceiver and the same MMF. The link frequency response was measured for all fiber lengths employed in the experiment using the set-up with the 10 GHz photoreceiver bandwidth. The obtained total link bandwidth values were then used to estimate fiber bandwidth for each fiber length. The fiber bandwidths were later used to calculate the total bandwidth of the link while employing a theoretical 15 GHz bandwidth photoreceiver. The 3 dB bandwidths were extracted from a Gaussian fit to the measured data and used to estimate rise times for different fiber lengths. The ISI penalty estimated from the rise time values was then used to calculate the receiver sensitivity as a function of bit-rate. For the sensitivity

calculations, it is assumed that the dominant noise source is thermal noise, which is justified for received power levels below 0 dBm, before shot noise and VCSEL relative intensity noise start to dominate. The noise bandwidth is assumed to be equal to the receiver bandwidth. This model and the assumptions are fully outlined in [28]. In the case of a Gaussian frequency response, the total bandwidth of the system,  $BW_{tot}$ , can be estimated from the bandwidth of each component as

$$BW_{tot}^{-2} \approx BW_{rec}^{-2} + BW_{las}^{-2} + BW_{fib}^{-2}, \quad (2)$$

where  $BW_{rec}$ ,  $BW_{las}$ , and  $BW_{fib}$  represent receiver, laser, and fiber bandwidths, respectively. Using the known values for  $BW_{rec}$  and  $BW_{las}$ , the value of  $BW_{fib}$  was estimated from Equation (2) and was later used to approximate the  $BW_{tot}$  for the case of the theoretical photoreceiver with 15 GHz bandwidth. This provides an estimate of system performance when using a photoreceiver with higher bandwidth. Although the real systems may not have a Gaussian response, this model simplifies the overall system behavior with an acceptable accuracy. Sensitivities at  $BER=10^{-12}$  were calculated for a range of bit-rates for BTB and different fiber lengths. This calculation was performed for the 10 GHz bandwidth photoreceiver employed in the experiment and also for a theoretical 15 GHz bandwidth photoreceiver to investigate the effect of limited receiver bandwidth on the performance. Calculated and measured sensitivity values at 20, 22, and 25 Gb/s are summarized in Table I, where it is evident that the difference between calculated and measured values are less than 0.5 dB for all cases, except the case of 800 m at 20 Gb/s. The lower calculated sensitivity for the 1100 m fiber case, compared to the 800 m case, arises from the higher measured system bandwidth for the 1100 m case, which is in agreement with the 22 Gb/s BER measurement shown in the previous section. The calculated sensitivities using the theoretical 15 GHz photoreceiver are also given in Table I for different fiber lengths at 20, 22, and 25 Gb/s.

TABLE I  
MEASURED AND CALCULATED SENSITIVITY VALUES AT  $BER=10^{-12}$

		BTB	500m	800m	1.1km
10GHz real receiver	20G meas.	-9.6	-9.3	-8.4	-7.7
	20G calc.	-9.7	-8.9	-7.2	-7.8
	22G meas.	-8.6	-8.2	-6.0	-6.7
	22G calc.	-8.8	-7.8	-5.6	-6.4
	25G meas.	-7.2	-6.1	-	-
	25G calc.	-7.3	-5.9	-2.2	-3.6
15GHz theoretical receiver	20G calc.	-10.7	-9.9	-8.3	-8.8
	22G calc.	-10.2	-9.3	-7.2	-7.9
	25G calc.	-9.4	-8.2	-5.4	-6.4

Sensitivity values are given in dBm.

As expressed in the table, utilizing a 15 GHz receiver improves sensitivities by 1-2 dB for all bit-rates. This is a result of reduced ISI. It is also evident that the calculated receiver sensitivities with the 15 GHz receiver at 25 Gb/s are almost equal to, or better than, the case with the 10 GHz receiver at 22 Gb/s. This indicates that by employing a 15 GHz receiver one can achieve data transmission over ~1 km of MMF at 25 Gb/s using the quasi-single mode VCSEL and OM4 fiber.

The calculations for a 2 km link showed that a

photoreceiver with higher than 15 GHz bandwidth is required to achieve a sensitivity of  $<-6$  dBm for 20 Gb/s data-transmission over 2 km of MMF. To increase the reach at high bit-rates (25 Gb/s in this case), the VCSEL power should be high enough to overcome the connector and fiber losses and effects of fiber dispersion to reach the required receiver sensitivity levels for the error-free detection. Moreover, VCSELs with narrower spectral width (smaller number of transverse modes) are favorable to reduce the effects of chromatic and modal dispersion in the fiber. This renders a higher effective bandwidth for the fiber which can alter the overall system performance, in particular when it is not limited by the receiver bandwidth. However, one should also consider larger modal noise in the links employing MMFs and higher coherence, narrow spectral width VCSELs resulting from interference between fiber modes and mode selective loss in the link [29].

## V. CONCLUSION

High-speed, small aperture VCSELs for extended reach data communication at high bit-rates were presented. The small oxide aperture ( $\sim 3$   $\mu\text{m}$ ) and the reduced top DBR reflectivity led to a narrow spectral width (0.29 nm) for high fiber bandwidth, high slope efficiency for efficient modulation, a high output power (2 mW) to overcome power loss during transmission over long lengths of fiber, and a high modulation bandwidth (21 GHz) for transmission at high bit-rates. This enabled error-free data transmission over more than 1 km of OM4 MMF at bit-rates exceeding 20 Gb/s. Data transmission at 20, 22, and 25 Gb/s over different fiber lengths and a corresponding theoretical analysis revealed that the achievable bit-rate at long transmission distances was limited by the bandwidth of the photoreceiver used in the experiment. Calculations with a theoretical photoreceiver bandwidth of 15 GHz showed a significant improvement of the receiver bandwidth due to reduced ISI which should allow for 25 Gb/s data transmission over 1 km of MMF using these VCSELs. Employing quasi-single mode VCSELs with even higher output power and narrower spectral width will enable transmission over even longer MMFs.

## ACKNOWLEDGMENT

The authors would like to thank IQE Europe Ltd. for providing the epitaxial growth.

## REFERENCES

- [1] C. F. Lam, H. Liu, B. Koley, X. Zhao, V. Kamalov, and V. Gill, "Fiber Optic Communication Technologies: What's Needed for Datacenter Network Operations," *IEEE Communications Magazine*, vol. 48, no. 7, pp. 32–39, Jul. 2010.
- [2] H. Liu, C. F. Lam, and C. Johnson, "Scaling Optical Interconnects in Datacenter Networks Opportunities and Challenges for WDM," *18th IEEE Symposium on High Performance Interconnects (HOTI)*, pp. 113–116, 2010.
- [3] A. Larsson, "Advances in VCSELs for Communication and Sensing," *IEEE Journal of Selected Topics in Quantum Electronics*, vol. 17, no. 6, pp. 1552–1567, Dec. 2011.
- [4] M. A. Taubenblatt, "Optical Interconnects for High-Performance Computing," *Journal of Lightwave Technology*, vol. 30, no. 4, pp. 448–457, Feb. 2012.
- [5] J. B. Schlager, M. J. Hackert, P. Pepejugoski, and J. Gwinn, "Measurements for Enhanced Bandwidth Performance Over 62.5- $\mu\text{m}$  Multimode Fiber in Short-Wavelength Local Area Networks," *Journal of Lightwave Technology*, vol. 21, no. 5, pp. 1276–1285, May 2003.
- [6] A. Gholami, D. Molin, and P. Sillard, "Compensation of Chromatic Dispersion by Modal Dispersion in MMF- and VCSEL-Based Gigabit Ethernet Transmissions," *IEEE Photonics Technology Letters*, vol. 21, no. 10, pp. 645–647, Jun. 2009.
- [7] R. E. Freund, C.-A. Bunge, N. N. Ledentsov, D. Molin, and C. Caspar, "High-Speed Transmission in Multimode Fibers," *Journal of Lightwave Technology*, vol. 28, no. 4, pp. 569–586, Feb. 2010.
- [8] P. Pepejugoski, D. Kuchta, Y. Kwark, P. Pleunis, and G. Kuyt, "15.6-Gb/s Transmission Over 1 km of Next Generation Multimode Fiber," *IEEE Photonics Technology Letters*, vol. 14, no. 5, pp. 717–719, May 2002.
- [9] P. Westbergh, R. Safaisini, E. Haglund, J. S. Gustavsson, A. Larsson, M. Geen, R. Lawrence, and A. Joel, "High-Speed Oxide Confined 850-nm VCSELs Operating Error-Free at 40 Gbit/s up to 85°C," *IEEE Photonics Technology Letters*, submitted for publication.
- [10] E. Haglund, Å. Haglund, P. Westbergh, J. S. Gustavsson, B. Kögel, and A. Larsson, "25 Gbit/s transmission over 500 m multimode fibre using 850 nm VCSEL with integrated mode filter," *Electronics Letters*, vol. 48, no. 9, pp. 517–518, Apr. 2012.
- [11] J. A. Lott, A. S. Payusov, S. A. Blokhin, P. Moser, and D. Bimberg, "Arrays of 850 nm photodiodes and vertical cavity surface emitting lasers for 25 to 40 Gbit/s optical interconnects," *Physica Status Solidi C*, vol. 9, no. 2, pp. 290–293, 2011.
- [12] P. Moser, J. A. Lott, P. Wolf, G. Larisch, H. Li, N. N. Ledentsov, and D. Bimberg, "56 fJ dissipated energy per bit of oxide-confined 850 nm VCSELs operating at 25 Gbit/s," *Electronics Letters*, vol. 48, no. 20, pp. 1292–1294, Sep. 2012.
- [13] G. Fiol, J. A. Lott, N. N. Ledentsov, and D. Bimberg, "Multimode optical fibre communication at 25 Gbit/s over 300 m with small spectral-width 850 nm VCSELs," *Electronics Letters*, vol. 47, no. 14, pp. 810–811, Jul. 2011.
- [14] P. Moser, J. A. Lott, P. Wolf, G. Larisch, A. Payusov, N. Ledentsov, and D. Bimberg, "Energy-Efficient Oxide-Confined 850 nm VCSELs for Long Distance Multimode Fiber Optical Interconnects," *IEEE Journal of Selected Topics in Quantum Electronics*, no. 99, 2012.
- [15] R. Safaisini, K. Szczerba, E. Haglund, P. Westbergh, J. S. Gustavsson, A. Larsson, and P. A. Andrekson, "20 Gbit/s error-free operation of 850 nm oxide-confined VCSELs beyond 1 km of multimode fibre," *Electronics Letters*, vol. 48, no. 19, pp. 1225–1227, Sep. 2012.
- [16] G. Giarretta, R. Michalzik, and A. J. Ritger, "Long distance (2.8 km), short wavelength (0.85  $\mu\text{m}$ ) data transmission at 10 Gb/sec over new generation high bandwidth multimode fiber," *Conference on Lasers and Electro-Optics (CLEO)*, pp. 678–679, 2000.
- [17] B. M. Hawkins, R. A. Hawthorne, J. K. Guenter, J. A. Tatum, and J. R. Biard, "Reliability of various size oxide aperture VCSELs," in *Proc. 52<sup>nd</sup> Electronic Components and Technology Conference*, pp. 540–550, 2002.
- [18] P. Westbergh, J. S. Gustavsson, B. Kögel, Å. Haglund, and A. Larsson, "Impact of Photon Lifetime on High-Speed VCSEL Performance," *IEEE Journal of Selected Topics in Quantum Electronics*, vol. 17, no. 6, pp. 1603–1613, Dec. 2011.
- [19] S. B. Healy, E. P. O'Reilly, J. S. Gustavsson, P. Westbergh, Å. Haglund, A. Larsson, and A. Joel, "Active Region Design for High-Speed 850-nm VCSELs," *IEEE Journal of Quantum Electronics*, vol. 46, no. 4, pp. 506–512, Apr. 2010.
- [20] "IEEE Standard for Information Technology--Telecommunications and Information Exchange Between Systems--Local and Metropolitan Area Networks--Specific Requirements Part 3: Carrier Sense Multiple Access With Collision Detection (CSMA/CD) Access Method and Physical Layer Specifications - Section Four," *IEEE Std 802.3-2008 (Revision of IEEE Std 802.3-2005)*, pp. 1–586, Dec. 2008.

- [21] P. Westbergh, J. S. Gustavsson, B. Kögel, Å. Haglund, A. Larsson, and A. Joel, "Speed enhancement of VCSELs by photon lifetime reduction," *Electronics Letters*, vol. 46, no. 13, pp. 938–940, Jun. 2010.
- [22] J. S. Gustavsson, A. Haglund, J. Bengtsson, P. Modh, and A. Larsson, "Dynamic behavior of fundamental-mode stabilized VCSELs using shallow surface relief," *IEEE Journal of Quantum Electronics*, vol. 40, no. 6, pp. 607–619, Jun. 2004.
- [23] O. Kjebon, R. Schatz, S. Lourdudoss, S. Nilsson, and B. Stalnacke, "Modulation response measurements and evaluation of MQW InGaAsP lasers of various designs," *Proc. SPIE*, vol. 2684, pp. 138–152, 1996.
- [24] L. Coldren and S. Corzine, *Diode Lasers and Photonic Integrated Circuits*. New York: Wiley, 1995.
- [25] Y. Ou, J. S. Gustavsson, P. Westbergh, Å. Haglund, A. Larsson, and A. Joel, "Impedance Characteristics and Parasitic Speed Limitations of High Speed 850-nm VCSELs," *IEEE Photonics Technology Letters*, vol. 21, no. 24, pp. 1840–1842, Dec. 2009.
- [26] P. Westbergh, R. Safaisini, E. Haglund, B. Kögel, J. S. Gustavsson, A. Larsson, M. Geen, R. Lawrence, and A. Joel, "High-speed 850 nm VCSELs with 28 GHz modulation bandwidth operating error-free up to 44 Gbit/s," *Electronics Letters*, vol. 48, no. 18, pp. 1145–1147, Aug. 2012.
- [27] P. Pepeljugoski, S. E. Golowich, A. J. Ritger, P. Kolesar, and A. Risteski, "Modeling and Simulation of Next-Generation Multimode Fiber Links," *Journal of Lightwave Technology*, vol. 21, no. 5, pp. 1242–1255, May 2003.
- [28] K. Szczerba, P. Westbergh, J. Karout, J. Gustavsson, Å. Haglund, M. Karlsson, P. Andrekson, E. Agrell, and A. Larsson, "4-PAM for High-Speed Short-Range Optical Communications," *Journal of Optical Communications and Networking*, vol. 4, no. 11, pp. 885–894, Nov. 2012.
- [29] D.M. Kuchta and C.J. Mahon, "Mode selective loss penalties in VCSEL optical fiber transmission links", *IEEE Photonics Technology Letters*, vol. 6, no. 2, pp. 288–290, 1994.